Electronic Supplementary Material (ESI) for Journal of Materials Chemistry A.
This journal is © The Royal Society of Chemistry 2020

Supporting Information

Defect-rich bimetallic yolk-shell metal-cyanide framework as efficient electrocatalyst for oxygen evolution reaction

Yongqiang Feng,[a] Peipei Dong,[a] Liyun Cao,[a] Xiao Wang,[a] Jia Wang,[b,c] Hai Wang,[a] Weihang Feng,[a] Junsheng Chen,[a] Liangliang Feng,[a] Chaozheng He,*[b,c] and Jianfeng Huang[a]*

Contents

almost identical to the pristine CoCo-PBA. YS-PBA-16 with a phase of $Co_2Fe^{II}(CN)_6$ but less defects exhibited an OER performance between YS-PBA and SC-PBA.

Figure S10. The top view (a) and side view (b) of the optimized structure for PBA. The blue and gold balls represent Fe and Co atoms, respectively, and the white and brown colored atoms represent N and C atoms, respectively. The atom enclosed by the red dotted line represents the removed Co atom.

Table S1. The OER properties of YS-PBA compared with other non-precious metal-based OER catalysts in 1 M KOH.

Additional data:

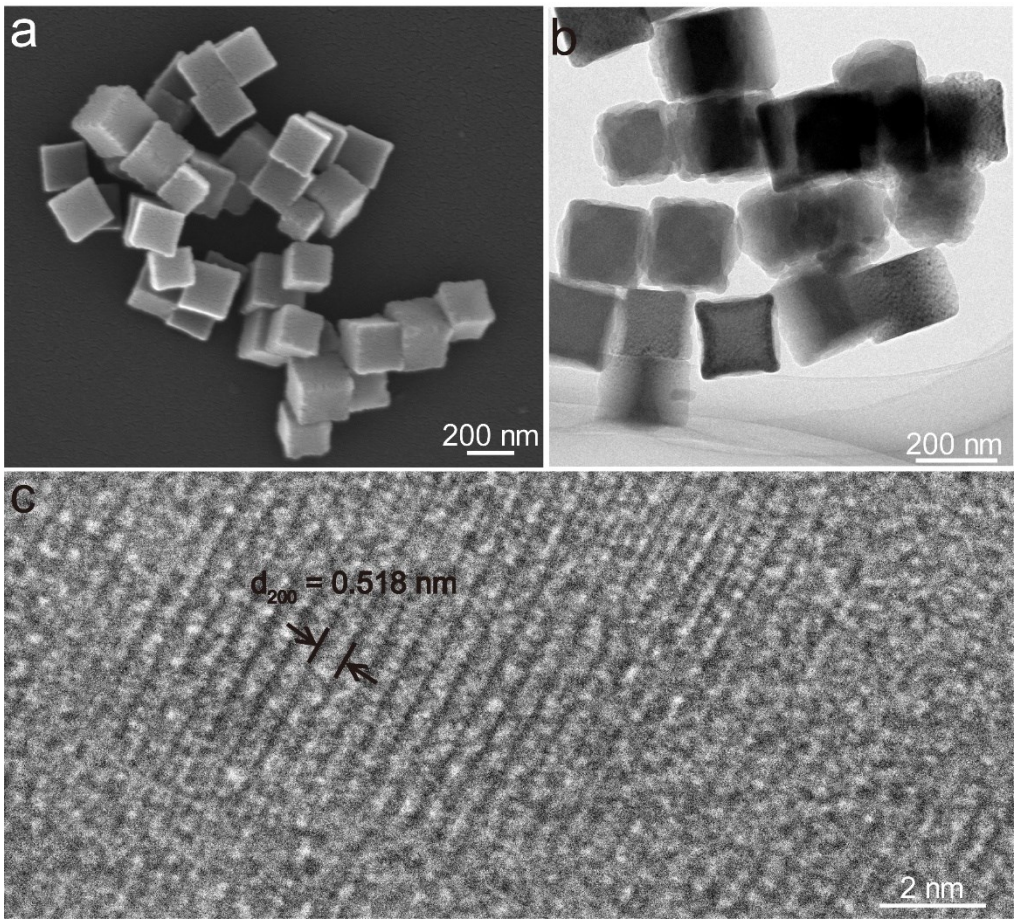

Figure S1. Morphology of the as-synthesized SC-PBA. (a) SEM, (b) TEM and (c) HRTEM.

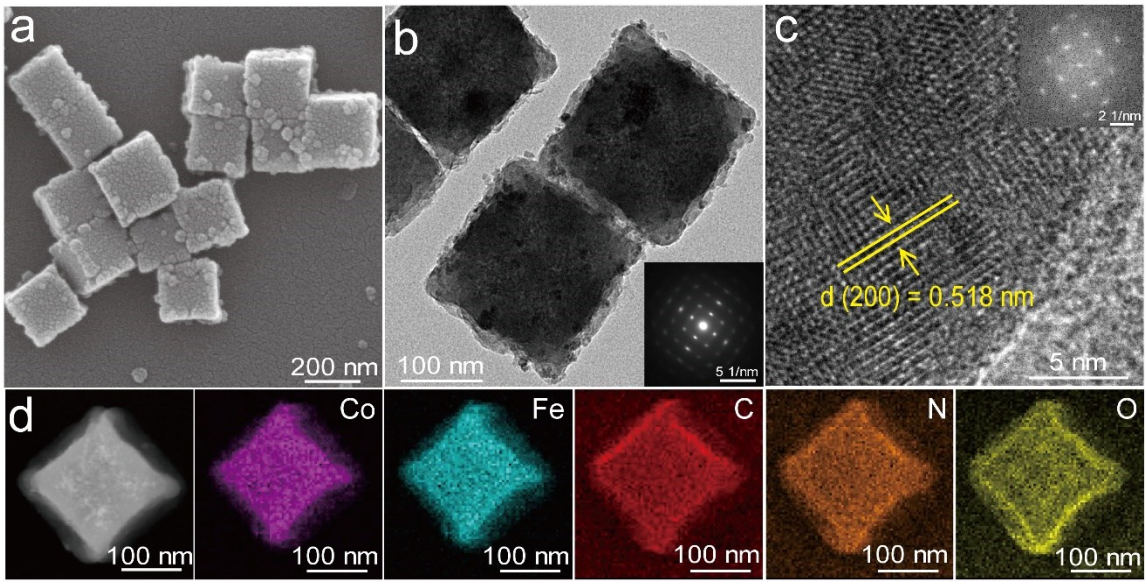

Figure S2. Morphology of SC-PBA after the solvothermal reaction under the simalar condition as YS-PBA except for the addition of PVP. (a) SEM, (b) TEM, inset: SAED, (c) HRTEM showing the typical fringe spacing of 0.518 nm in SC-PBA, indicating no phase transformation, and (d) the corresponding elemental mapping for Co, Fe, C, N, O.

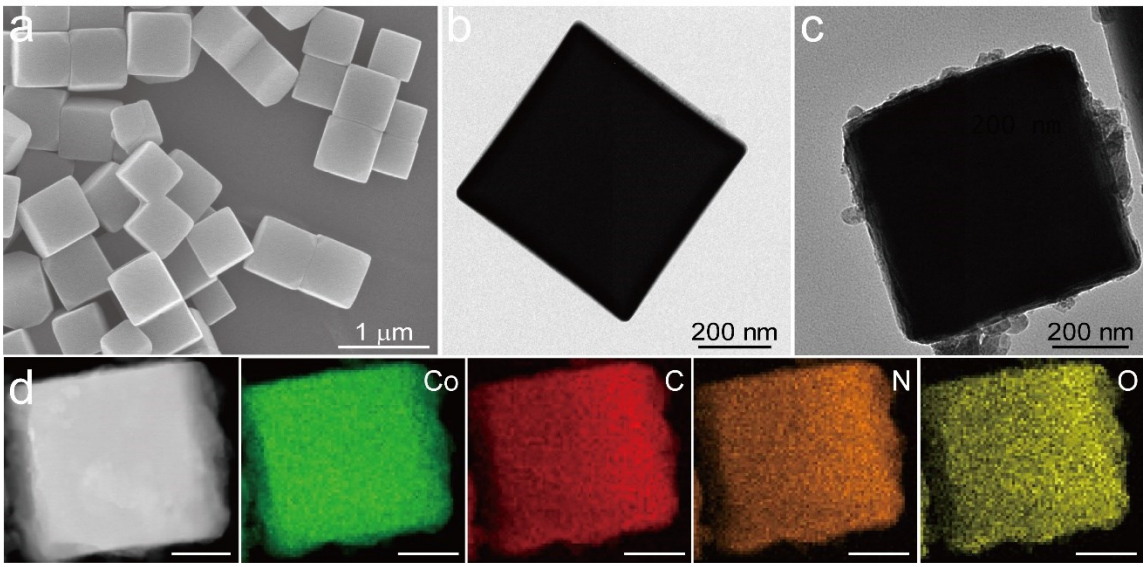

Figure S3. Morphology of CoCo-PBA. (a) SEM, (b) TEM of CoCo-PBA before the solvothermal reaction, (c) TEM and (d) the corresponding elemental mapping of CoCo-PBA after the solvothermal reaction (scale bar: 200 nm). The result indicated that no phase transformation was occured.

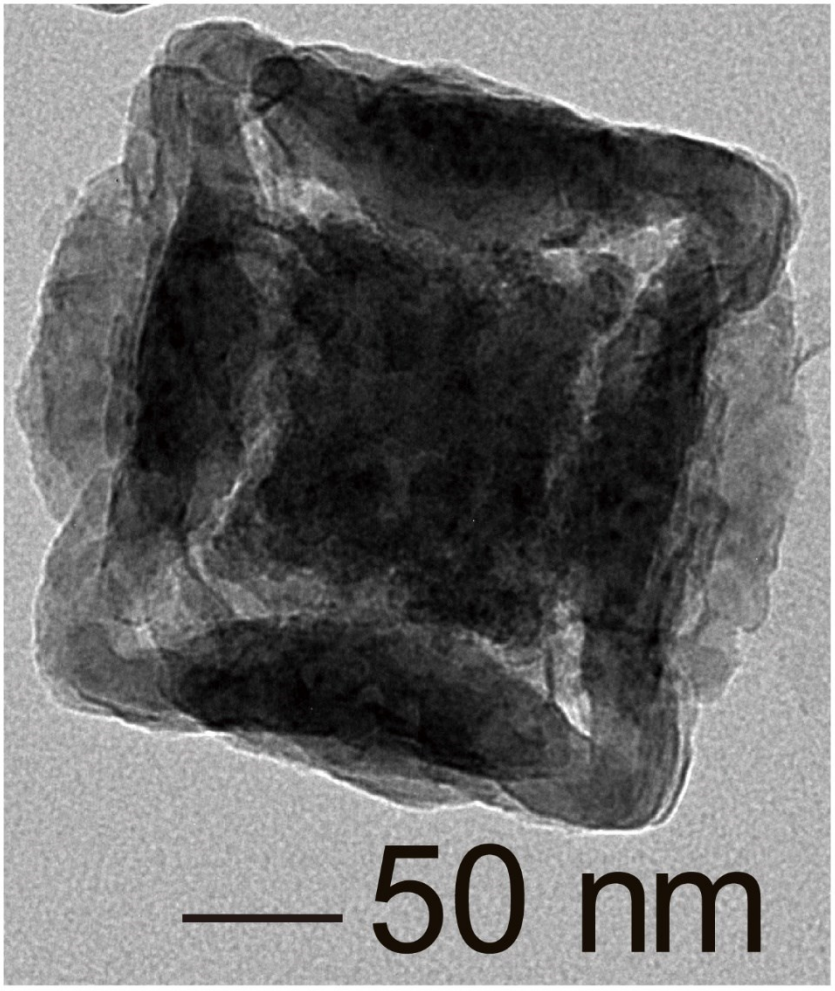

Figure S4. TEM image of YS-PBA after long-term chronoamperometry measurement.

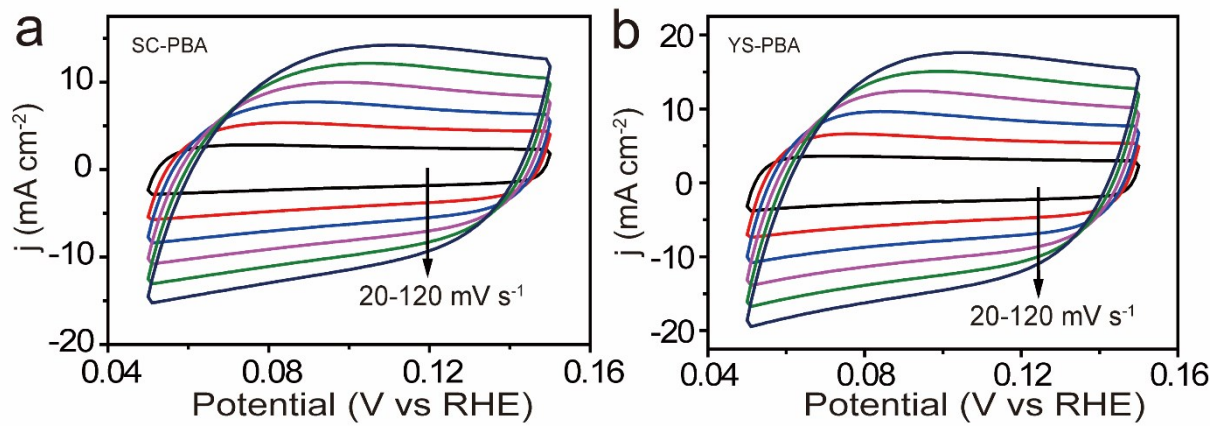

Figure S5. CV curves of SC-PBA (a) and YS-PBA (b) at a scan rate of 20, 40, 60, 80, 100 and 120 mV s^{-1} in 1 M KOH.

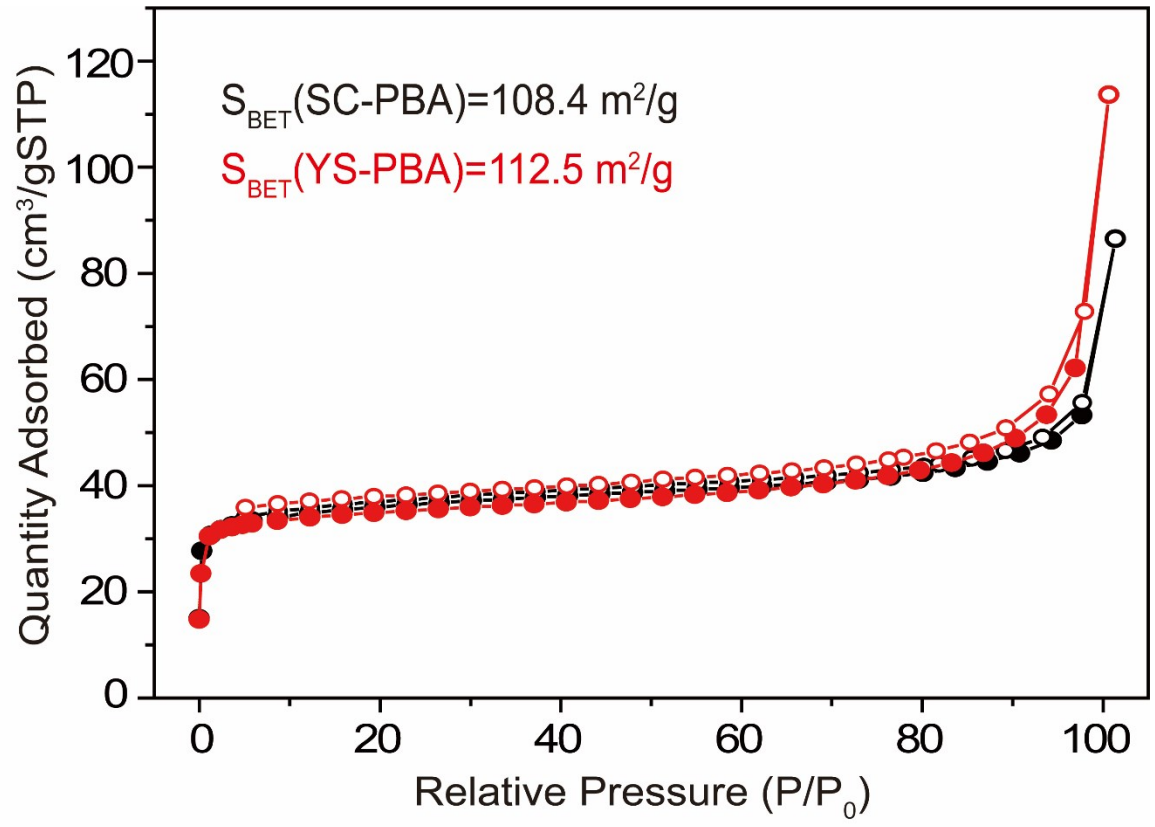

Figure S6. N_2 adsorption/desorption curves of SC-PBA (black) and YS-PBA (red) measured at 77 K.

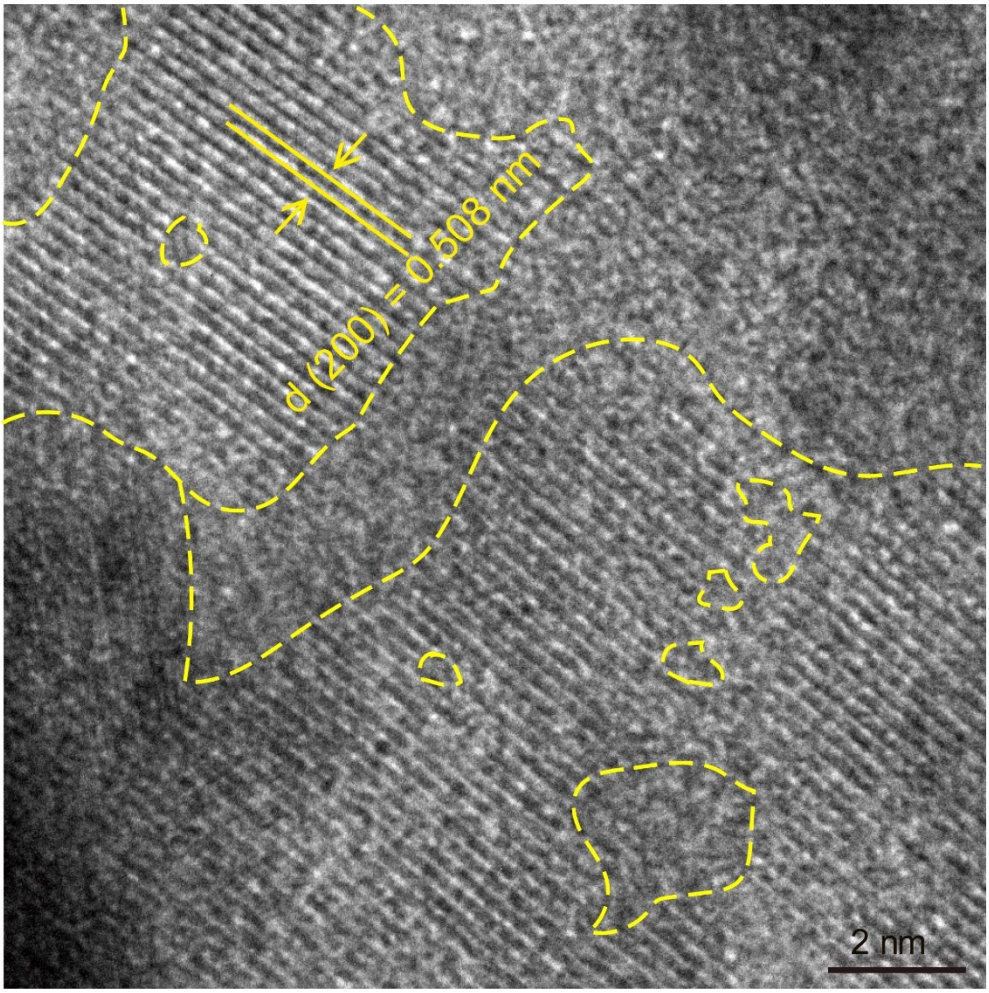

Figure S7. HRTEM of YS-PBA showing amorphous domains within the crystal lattice.

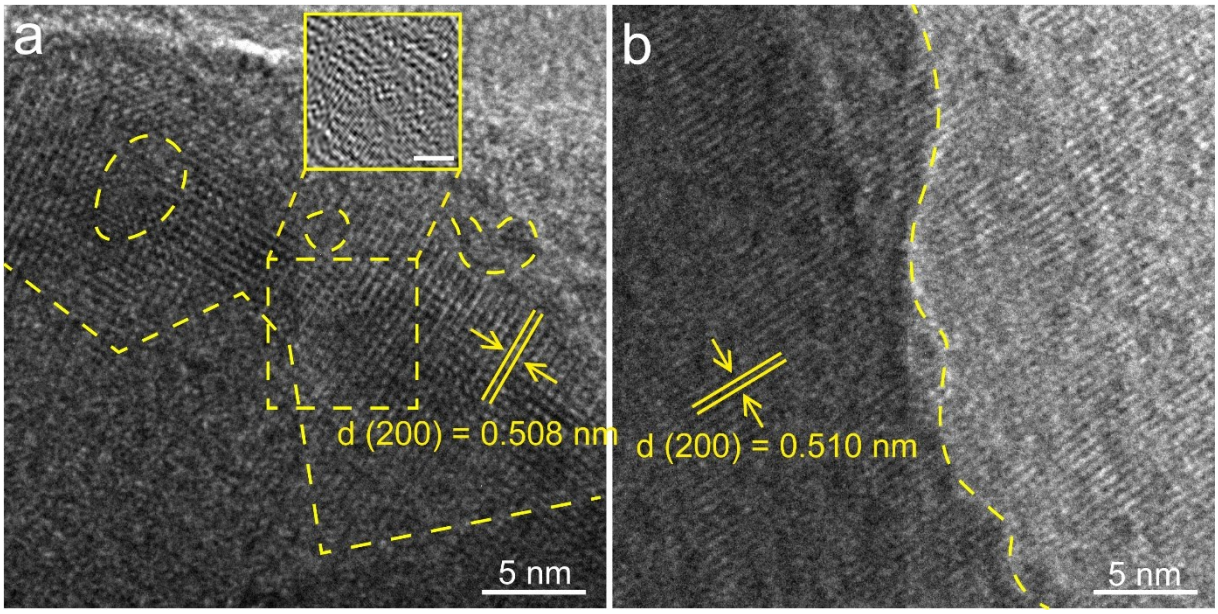

Figure S8. HRTEM of the core (a) and the shell (b) moieties of YS-PBA after i-t measurement. The atomic steps and boundaries could be observed as marked by yellow dashed lines, and the amorphous domains were labeled by yellow circles. The inset of (a) displayed the crystal dislocation of the marked area (scale bar: 2 nm).

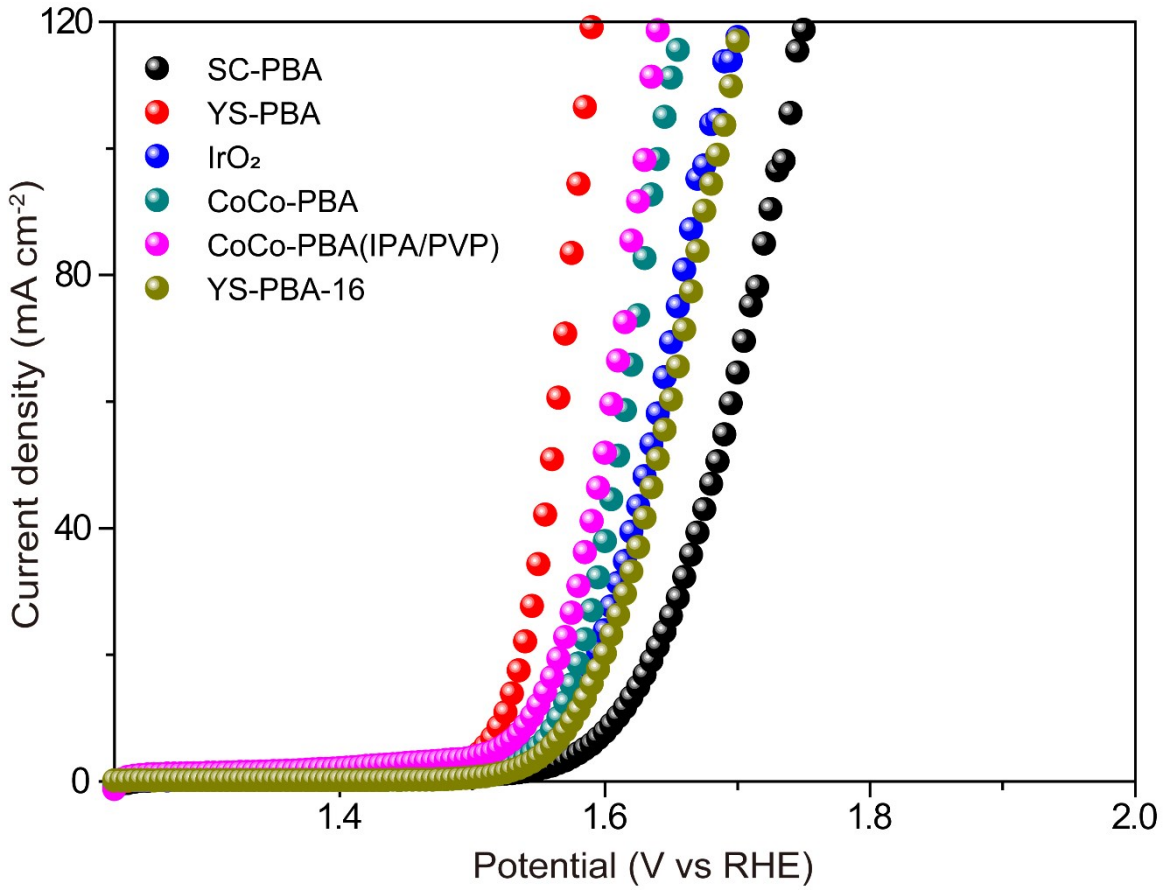

Figure S9. LSV curves of SC-PBA, YS-PBA, IrO_2, CoCo-PBA, CoCo-PBA(IPA/PVP) and YS-PBA-16. The OER activity of defect-free CoCo-PBA treated by IPA/PVP couple was almost identical to the pristine CoCo-PBA. YS-PBA-16 with a phase of $Co_2Fe^{II}(CN)_6$ but less defects exhibited an OER performance between YS-PBA and SC-PBA.

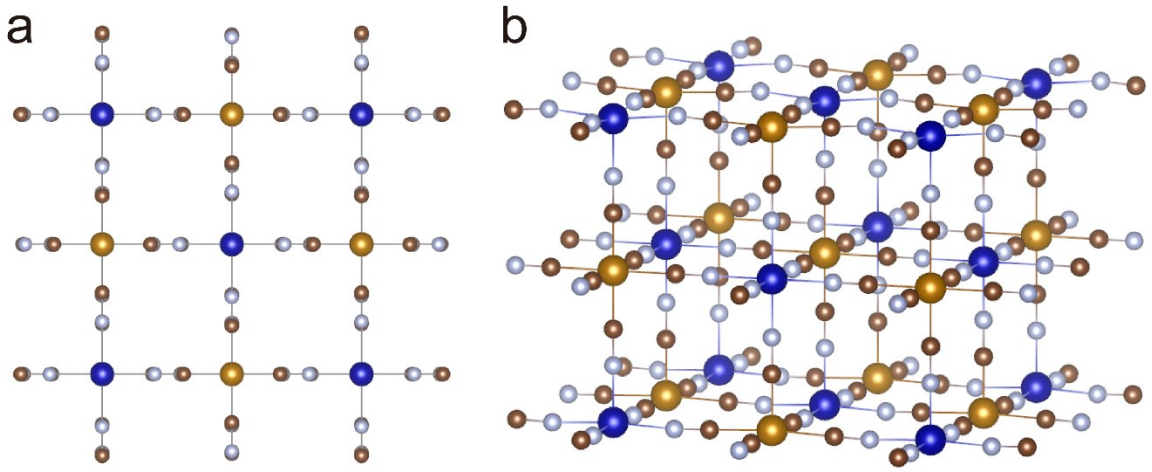

Figure S10. The top view (a) and side view (b) of the optimized structure for PBA. The blue and gold balls represent Fe and Co atoms, respectively, and the white and brown colored atoms represent N and C atoms, respectively. The atom enclosed by the red dotted line represents the removed Co atom.

Table S1. The OER properties of YS-PBA compared with other non-precious metal-based OER catalysts in 1 M KOH.

Catalysts	η_{10} (mV)	References
YS-PBA	293	This work
CoP/NCNHP	310	J. Am. Chem. Soc., 2018, 140, 2610-2618.
Co-Fe oxides NAFSs	340	Sci. Adv., 2017, 3, e1700732.
Co-Fe-O boxes	310	Chem, 2018, 4, 1967-1982.
$CoSe_2$ nanosheets	320	J. Am. Chem. Soc., 2014, 136, 15670-15675.
Co_3O_4-B	318	Adv. Energy Mater., 2014, 4, 1400696.
Ni-Co oxide cage	380	Adv. Mater., 2016, 28, 4601-4605.
CHFC	330	Sci. Rep., 2019, 9, 15965.
Co-N/GF-700	313	ACS Catal., 2018, 8, 4637-4644.
NiCoP/C	330	Angew. Chem. 2017, 129, 3955-3958
Exfoliated NiCo LDH	367	Nat. Commun. 2014, 5, 4477
CoMn LDH	324	J. Am. Chem. Soc. 2014, 136, 16481-16484